

bandwidth wider than 3.1–10.6 GHz with four notched bands four notched bands centered on 2.4, 3.5, 5.2, and 5.8 GHz. Meanwhile, it keeps omnidirectional radiation performance and stable gain successfully.

ACKNOWLEDGMENTS

This work is supported by the NSFC under contract No.61101066 and the Fundamental Research Funds for the Central Universities, and partially supported by the Program for New Century Excellent Talents in University of China, the NSFC under contract No.61072017, Natural Science Basic Research Plan in Shaanxi Province of China (No.2010JQ8013), and Foundation for the Returned Overseas Chinese Scholars, State Education Ministry and Shaanxi Province.

REFERENCES

1. Federal Communication Commission, First Report and Order, Revision of Part 15 of the Commission's Rule Regarding Ultra-Wideband Transmission systems FCC 02-48, 2002.
2. W.S. Lee, W.G. Lim, and J.W. Yu, Multiple band-notched planar monopole antenna for multiband wireless systems, *IEEE Microwave Wireless Compon Lett* 15 (2005), 576–578.
3. S.H. Lee, J.W. Baik, and Y.S. Kim, A coplanar waveguide fed monopole ultra-wideband antenna having band-notched frequency function by two folded-striplines, *Microwave Opt Technol Lett* 49 (2007), 2747–2750.
4. L. Liu, Y.Z. Yin, C. Jie, J.P. Xiong, and Z. Cui, A compact printed antenna using slot-type CSRR for 5.2 GHz/5.8 GHz band-notched UWB application, *Microwave Opt Technol Lett* 50 (2008), 3239–3242.
5. M.C. Tang, S.Q. Xiao, T.W. Deng, D. Wang, J. Guan, B.Z. Wang, and G.D. Ge, Compact UWB Antenna With Multiple Band-Notches for WiMAX and WLAN, *IEEE Trans Antennas Propag* 59 (2011), 1372–1376.

© 2012 Wiley Periodicals, Inc.

MODELING A SIW FILTER WITH IRIS WINDOWS USING EQUIVALENT CIRCUITS

Miguel Angel Tlaxcalteco-Matus and Reydezel Torres-Torres

Department of Electronics, National Institute for Astrophysics, Optics and Electronics—INAOE, A. P. 51 & 216, 72000, Puebla, Mexico; Corresponding author: mtlaxcalteco@inaoep.mx

Received 9 March 2012

ABSTRACT: A model and parameter extraction method for a substrate integrated waveguide (SIW) filter is presented. The proposed approach is derived from an analysis of full-wave simulations, allowing to obtain the equivalent circuit parameters for the iris. The accuracy of the method is demonstrated through a careful model–experiment correlation, allowing the correct representation of the SIW filter over the complete useful bandwidth. © 2012 Wiley Periodicals, Inc. *Microwave Opt Technol Lett* 54:2865–2868, 2012; View this article online at wileyonlinelibrary.com. DOI 10.1002/mop.27183

Key words: substrate integrated waveguide; filter; iris; unit cell; equivalent circuit

1. INTRODUCTION

Substrate integrated waveguides (SIW) serve as high-speed interconnects, multiport junctions, antennas, circulators, couplers, resonators, and filters [1–3]. In this regard, periodic struc-

tures compatible with SIW technology can be used to generate electromagnetic bandgaps [4]. These SIW filters create a rejection band around some central resonant frequency, which depends on the effective width of the SIW [1, 4]. Figure 1 shows three structures used for generating a SIW filter. The ideal structure is depicted in Figure 1(a), where the sidewalls are metal plates forming a waveguide varying in width along its length. In this case, each one of the sections where the width is reduced is referred to as iris. Thus, the dimensions and the total number of irises along the SIW determine the corresponding transfer function. Unfortunately, the structure in Figure 1(a) is not compatible with conventional PCB technology. Alternatively, other structures have been proposed such as that shown in Figure 1(b), which uses drilled metallic vias to emulate metallic sidewalls [4]. However, even though this structure is compatible with PCB technology, the relatively small size of the required drilled vias raises the fabrication cost. For this reason, a second alternative can be seen in Figure 1(c) [1, 5]. In this structure, the change in width along the SIW structure is achieved by using vias with a considerable bigger diameter than in the previous case, which makes it a more cost-effective solution.

The appropriate modeling of the structure shown in Figure 1(c) is necessary for carrying out a systematic selection of dimensions and materials for particular applications. In fact, these types of structures are commonly modeled using multiple unit cells that are concatenated [4–6]. However, current approaches require *a priori* knowledge of the material properties and the effective dimensions of the structures [7], which considerably complicates the modeling.

To represent the behavior of an SIW filter, the iris section depicted in Figure 1(d) is modeled using the equivalent circuit shown in Figure 1(e). Thus, in this article, an approach for systematically extracting the corresponding parameters is presented. In this case, the proposal allows to obtain the electrical components associated to an iris cell, and the inductance related to the change in the width of the SIW. Excellent agreement between the model and *S*-parameter measurements is observed within the useful bandwidth of the filter when applying the proposed method.

2. DESCRIPTION OF THE INVESTIGATED STRUCTURES

For the development and verification of the proposed methodology, two different SIW filters were fabricated on a PCB made

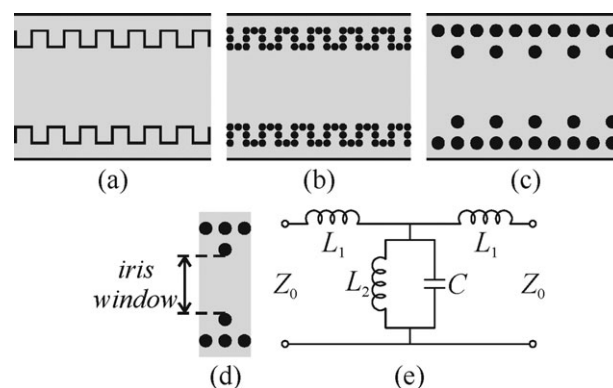


Figure 1 Sketches for three different implementations of an SIW filter: (a) using solid sidewalls, (b) using small ground vias, and (c) using large ground vias. The unit cell using for the third case and the corresponding model are shown in (d) and (e), respectively

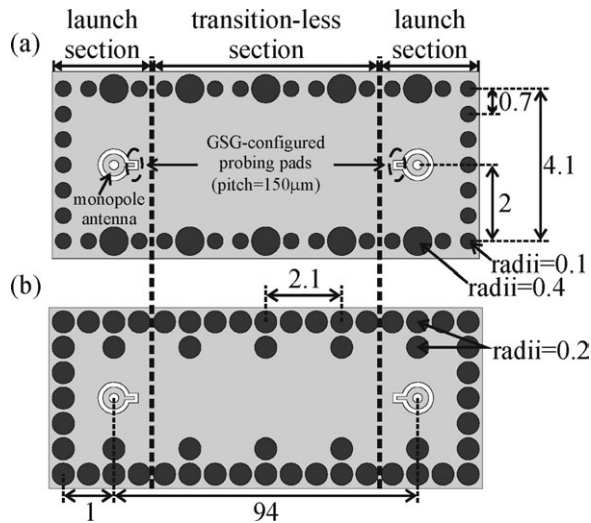


Figure 2 Layouts for the SIW filters presenting: (a) in-line scattering vias, and (b) off-line scattering vias (all the dimensions are given in millimeters)

of Rogers RT/Duroid 5880 material with a thickness of 0.79 mm. The nominal relative permittivity and loss tangent for this material at 50 GHz are $\epsilon_r = 2.2$ and $\tan\delta = 0.0017$, respectively. The details of the layout for the fabricated structures are shown in Figure 2. Notice that two types of structures were fabricated: (a) modulating the iris width by increasing the size of the vias (referred to as in-line vias) at the desired location, and (b) modulating the iris width by placing additional ground vias (referred to as off-line vias) at the desired location. Figures 2(a) and 2(b) show simplified sketches for both cases. In reality, the total number of irises is 67.

For the fabricated structures, additional vias acting as monopole antennas are used as launch structures, which are terminated with ground-signal-ground configured pads so that coplanar RF probes with a pitch of 150 μm can be used for measuring S -parameters with a previously calibrated vector network analyzer. These vias were designed to excite the single and dominant mode TE_{10} avoiding even modes. This allows to extend the usable transmission bandwidth from the cutoff frequency of the TE_{10} to the cutoff frequency of the TE_{30} , which is the next higher order odd mode.

3. MODELING AND PARAMETER DETERMINATION METHOD

In the model shown in Figure 1(e), the inductive element L_2 represents the change in width of the waveguide, whereas L_1 considers the interaction of a signal traveling through the waveguide with the posts of the iris window (i.e., the posts act as scatterers). Notice that the model presents also a capacitance C , which allows to take into account the dependence on frequency of the iris impedance due to the fact that the scatterer is not perfectly square [8]. Furthermore, because the width of the scatterer is relatively small, the effect of the iris can be concentrated at the middle of the unit cell.

As a first step for determining the elements in the model of Figure 1(e), a three-dimensional (3D) model was implemented for the unit cell in a full-wave simulator. The implemented 3D model for the unit cell is terminated with two additional sections of waveguide used to define the corresponding input and output ports. Thus, two different unit cells; one for the in-line and another for the off-line vias were designed in the same dielectric material as that assumed in the fabricated structures. The dimen-

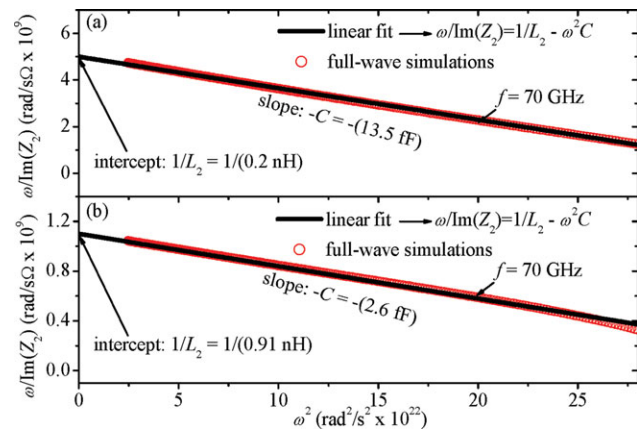


Figure 3 Regression for determining: L_2 and C for the SIW filters with: (a) off-line, and (b) in-line scattering vias. [Color figure can be viewed in the online issue, which is available at wileyonlinelibrary.com]

sions of the iris window are 2.3 and 3.3 mm, whereas the radii of the scatterers are 0.2 and 0.4 mm for the off-line and in-line vias, respectively. Once the simulated S -parameters are obtained, a deembedding process is applied to remove the effect of the sections of waveguide that are added to perform the simulation. Afterwards, the inductances L_1 and L_2 , and the capacitance C can be obtained as follows. When converting the simulated S -parameters to Z -parameters, L_2 and C are obtained from the linear regression performed in Figure 3. Then, L_1 is obtained from the $\text{Im}(Z_{11} - Z_{12})/\omega$ versus ω^2 curve, where $\omega = 2\pi f$. Figure 4 shows the determination of L_1 , which presents a negative value due to the dispersion of evanescent modes in the iris [9]. As can be seen in Figure 5, the equivalent circuit for the unit cell accurately reproduces the full-wave simulations corresponding to the reflection and transmission parameters (i.e., S_{11} and S_{21} , respectively) for both analyzed structures.

Notice in Figure 5 that the rejection band is not observed in $|S_{21}|$ because these curves correspond to a single cell, and it is well known that the bandgap not only depends on the modulation of the iris window, but also on the number of unit cells concatenated in the structure [4]. In fact, the magnitude of the rejection increases as the number of cells in cascade connection increases. Moreover, this magnitude is also affected by changing the iris window. This can be clearly seen in Figure 6(a) where $|S_{21}|$ versus frequency data obtained from full-wave simulations

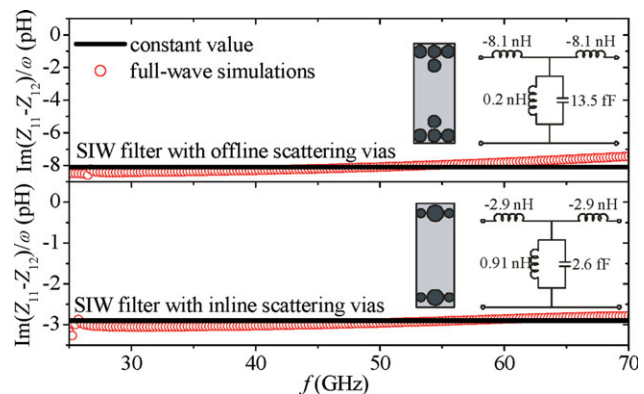


Figure 4 Determination of L_1 for the SIW filters with off-line, and in-line scattering vias. Insets: resulting circuits for the corresponding unit cells. [Color figure can be viewed in the online issue, which is available at wileyonlinelibrary.com]

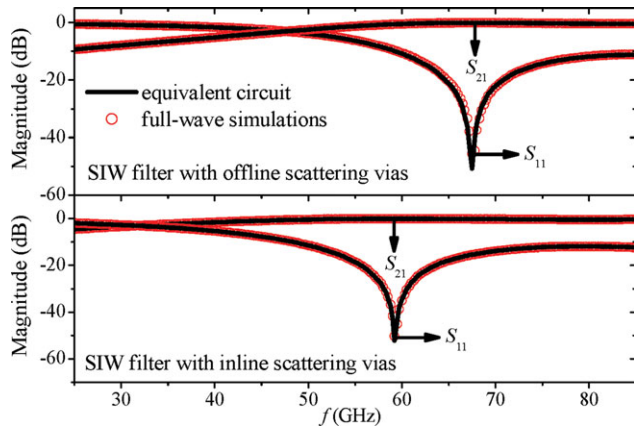


Figure 5 Comparison between the equivalent circuit model and full-wave simulations for the unit cell for the SIW filters with offline scattering vias, and inline scattering vias. [Color figure can be viewed in the online issue, which is available at wileyonlinelibrary.com]

are shown. Thus, each one of the curves presented in Figure 6(a) corresponds to 12 unit cells of the same size in cascade connection; for each curve, a different iris window is considered. To systematically observe the impact of varying the iris window on the characteristics of the SIW filter, the following analysis is carried out.

As a first approach, the frequency of resonance for the filter can be approximately determined from the transmission curves shown in Figure 6(a). However, the relative low rejection occurring when the iris window is small difficulties the precise calculation of this frequency. Nevertheless, $|Z_{11}|$ obtained from a conversion from S - to Z -parameters allows to accurately determine not only the cutoff frequency for the rejection band (i.e., f_{rb}) but also the cutoff frequency of the SIW itself (i.e., f_s). Figure 6(b) shows $|Z_{11}|$ for the six simulated structures. As can be seen, both frequencies, f_s and f_{rb} , are easily identified in this case. Notice that the impact of varying the iris window is more noticeable for f_s because the cutoff wavelength for allowing signal propagation is shorter as the effective width of the SIW is made smaller, whereas f_{rb} is more dependent on the periodicity of the scatterers.

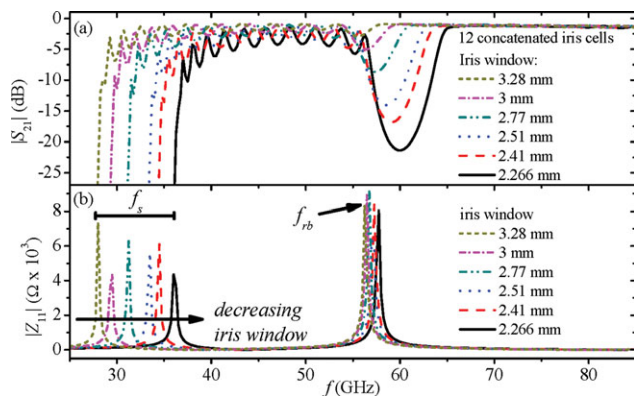


Figure 6 Corresponding simulations for the unit cells (a) comparison of the bandgap response for several iris window values, and (b) magnitude of Z_{11} obtained from the simulated unit cell when modulating the iris window. [Color figure can be viewed in the online issue, which is available at wileyonlinelibrary.com]

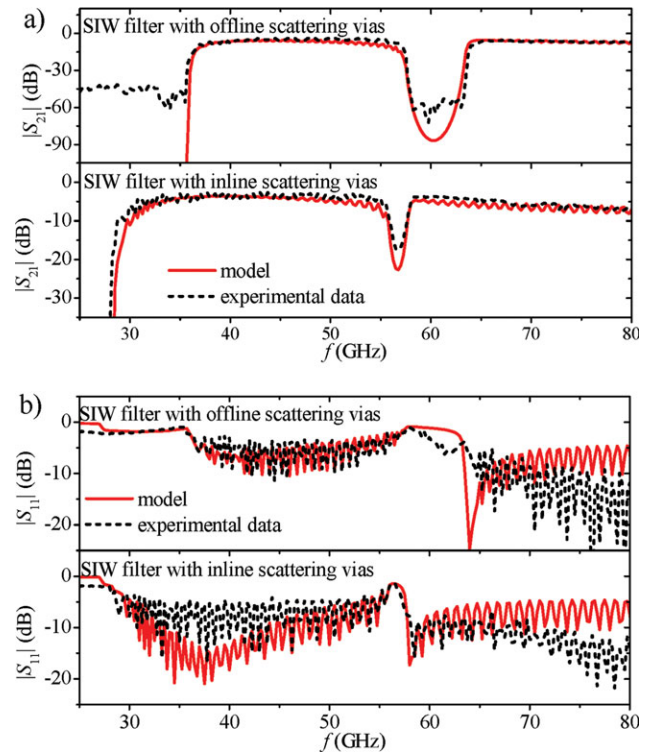


Figure 7 Comparison between the measured and simulated (a) insertion losses and (b) return losses for the fabricated SIW filters. [Color figure can be viewed in the online issue, which is available at wileyonlinelibrary.com]

4. EXPERIMENTAL VERIFICATION AND DISCUSSION

For the final implementation of the model for the structures depicted in Figure 2, the complete structures is assumed to include launch structures at each port of the structure [10]. In addition, the transitionless section composed by 67 concatenated iris-cells is represented by means of the corresponding equivalent circuits obtained in the previous section. Thus, the three main sections that conform the prototypes are completely represented with an equivalent circuit model. In this case, the complete structure can be simulated in a commercial circuit simulator; in this case, Agilent ADS.

Figure 7 shows the comparison between the measured S -parameters and the simulations using the proposed equivalent circuit for the fabricated structures. As can be seen, excellent simulation–experiment correlation is achieved in the complete useful bandwidth. Figure 7 also shows the impact of the modulation of the iris in response to the rejection band. As is mentioned in the previous section, the bandgap is broader if the iris window decreases. Because the offline structure presents additional ground vias for the scatterers, these scatterers penetrate more inside the structure causing a bigger dispersion of the electromagnetic fields at the frequency of interest. In addition, the use of extra ground vias allows to model the homogenous part of the SIW in a easy way (i.e., the effective width to obtain the complex propagation constant and the characteristic impedance). Nevertheless, the use of extra ground vias makes the inline configuration a cost-effective option.

5. CONCLUSIONS

A methodology for modeling SIW filters using capacitive and inductive elements has been presented and demonstrated. In addition to the inductive behavior of the iris modulation, the model for the interaction of the signal and the scatterers was

obtained and validated using full-wave simulations. Excellent agreement between simulated and experimental data was achieved for the transmission parameters within the entire useful bandwidth of the structures. Hence, the resulting modeling and parameter extraction technique allows for the representation of PCB-compatible SIW filters in a simple and straightforward way using equivalent circuits.

ACKNOWLEDGMENT

The authors would like to acknowledge Intel Co., for the fabrication of the devices. This work was partially supported by Intel Co., and CONACyT-Mexico under grants 227913 and 154337 respectively.

REFERENCES

1. G. Romo and A. Ciccomancini, Substrate integrated waveguide (SIW) filter: Design methodology and performance study, In: Proceeding of IEEE MTT-S IMW Symposium, February 2009, pp. 23–26.
2. M. Bozzi, L. Perregrini, and K. Wu, A novel technique for the direct determination of multimode equivalent circuit models for substrate integrated waveguide discontinuities, *Int. J RF Microw Comp Eng* 19 (2009), 423–433.
3. J. Simpson, A. Taflove, J. Mix, and H. Heck, Substrate integrated waveguides optimized for ultrahigh-speed digital interconnects, *IEEE Trans Microw Theory Tech* 54 (2006), 1983–1990.
4. J.D. Schwartz et al., Design and analysis of 1-D uniform and chirped electromagnetic bandgap structures in substrate-integrated waveguides, *IEEE Trans Microw Theory Tech* 58 (2010), 1858–1866.
5. A. Adabi and M. Tayarani, Substrate integration of dual inductive post waveguide filter, *Prog Electromagn Res B* 7 (2008), 321–329.
6. F. Mira, M. Bozzi, F. Giuppi, L. Perregrini, and A. Georgiadis, Efficient design of SIW filters by using equivalent circuit models and calibrated space-mapping optimization, *Int J RF Microw Comput Aided Eng* 20 (2010), 689–698.
7. X.P. Chen and K. Wu, Accurate and efficient design approach of substrate integrated waveguide filter using numerical TRL calibration technique, In: IEEE MTT-S International Microwave Symposium Digest 2008, pp. 1231–1234.
8. C.X. Zhou, Y.X. Guo, and S.L. Yan, Efficient design of SIW filters with knowledge-embedded space mapping technique, *Int J RF Microw Comput Aided Eng* 22 (2012), 603–609.
9. L. Lewin, A contribution to the theory of probes in waveguides, In: IEE Monograph, October 1957, pp. 109–116.
10. M. Tlaxcalteco-Matus and R. Torres-Torres, Systematic modeling and characterization of a via-to-SIW transition, *IEEE Microw Wirel Compon Lett* 20 (2010), 657–659.

© 2012 Wiley Periodicals, Inc.

TRANSMITTER FRONT-END WITH A NEW WIDEBAND ACTIVE BALUN IN 65-nm CMOS TECHNOLOGY

Kuan-Ting Lin,¹ Hsien-Ku Chen,¹ Tao Wang,² and Shey-Shi Lu¹

¹ Graduate Institute of Electronics Engineering, National Taiwan University, Taipei, Taiwan, Republic of China; Corresponding author: sslu@ntu.edu.tw

² Department of Electronic Engineering, Chang Gung University, Taoyuan, Taiwan, Republic of China

Received 16 March 2012

ABSTRACT: A 2.4 GHz transmitter front-end with a wideband active balun is proposed. The wideband active balun is able to work ideally by adopting a resistive compensation technique, which balances the gain of the differential input. In addition, a variable-gain preamplifier driver

with a dynamic range of 18 dB is utilized for the autogain loop control feature. The proposed wideband active balun only occupies $15 \times 27 \mu\text{m}^2$, which is profoundly small compared with conventional baluns and is promising in the differential to single signal conversion in wideband applications. © 2012 Wiley Periodicals, Inc. *Microw Opt Technol Lett* 54:2868–2871, 2012; View this article online at wileyonlinelibrary.com. DOI 10.1002/mop.27190

Key words: wideband; active balun; preamplifier driver; variable-gain amplifier; CMOS; transmitter; transformer

1. INTRODUCTION

A balun plays an important role in a low-power transmitter diagram, which connects the differential output of the up-converter to the single-ended power amplifier (PA). As a high-power-consuming component in a transceiver system, PA is usually designed in the single-ended topology for power efficiency [1]. Conventionally, a balun is composed of lumped devices [2] or transformers [3, 4], which consume a lot of chip area and are unable to realize a wideband characteristic due to their wavelength correspondence. Contrary to the passive balun, an active balun is able to consume much smaller area and exhibit a wideband response. An active balun can be realized with compound semiconductors such as P-HEMTs [5], but the power consumption can be as high as 370 mW. To resolve the power and size issues, an active balun with low power and small area is proposed and adopted in a transmitter front-end. From DC to 10 GHz, the proposed balun can provide a small gain mismatch of <0.9 dB and a phase-imbalance of $<1.2^\circ$. A resistive compensation technique is proposed to improve the balance of gain response to the differential input. Design equation of this compensating R_C is derived for the initial design.

2. TRANSMITTER FRONT-END CIRCUIT DESIGN

Figure 1 shows the schematic of whole transmitter front-end. The up-conversion mixer consists of a transconductance stage (M1–M2), switch pairs (M3–M6), and the resistive load R_L . As the Gilbert mixer is well-known, the discussion of this letter will be focused on the active balun and variable-gain preamplifier driver (VG-PAD) in Section 2.1. and 2.2., respectively.

2.1. Active Balun

Figure 2(a) shows the small-signal model of the proposed active balun. The frequency response of V_{OP} can be derived as follows:

$$V_{OP} = \frac{s^2 + s(\omega_{0,n}/Q_n) + \omega_{0,n}^2}{s^2 + s(\omega_{0,d}/Q_d) + \omega_{0,d}^2} \cdot V_{IP}, \quad (1)$$

where

$$\omega_{0,n} = \sqrt{g_{m7}/(C_{gs7}C_{gs10}R_G)} \quad (2)$$

$$Q_n = \sqrt{g_{m7}C_{gs7}C_{gs10}R_G/(g_{m7}C_{gs10}R_G + C_{gs7})} \quad (3)$$

$$\omega_{0,d} = \sqrt{(g_{m7} + g_{m10})/(C_{gs9}C_{gs10}R_G + C_{gs7}C_{gs9}R_G)} \quad (4)$$

$$Q_d = \frac{\sqrt{(g_{m7} + g_{m10})(C_{gs9}C_{gs10}R_G + C_{gs7}C_{gs10}R_G)}}{(C_{gs7} + C_{gs9} + C_{gs10} + g_{m7}C_{gs9}R_G)} \quad (5)$$

Furthermore, the output of the active balun V_{OM} can be calculated as: